ISSN 1029-9599, Physical Mesomechanics, 2019, Vol. 22, No. 4, pp. 275–286. © Pleiades Publishing, Ltd., 2019.
Russian Text © The Author(s), 2018, published in Fizicheskaya Mezomekhanika, 2018, Vol. 21, No. 2, pp. 33–44.

Direct Crystal Elastoviscoplasticity Model: An Application to the Study of Single Crystal Deformation

P. V. Trusov[1]*, A. Yu. Yanz[1], and L. A. Teplyakova[2]

[1] *Perm National Research Polytechnic University, Perm, 614990 Russia*
[2] *Tomsk State University of Architecture and Civil Engineering, Tomsk, 634003 Russia*
** e-mail: tpv@matmod.pstu.ac.ru*

Received November 11, 2017, revised December 28, 2017, accepted January 24, 2018

Abstract—This paper models the uniaxial compression of a single crystal of commercial purity aluminum, and compares the modeling results with experimental data. The problem is solved using a first-type direct model based on the finite element method. The material behavior is described by a crystal elastoviscoplasticity model that explicitly accounts for shearing on crystallographic planes. The main feature of this study is a physically sound description of the geometric nonlinearity associated with crystal lattice rotation. The modeling results show that the original homogeneous single crystal is divided into volumes with different plastic shear rate intensity and lattice orientation, which is in satisfactory agreement with experimental data.

DOI: 10.1134/S1029959919040039

Keywords: single crystal, geometric nonlinearity, crystal plasticity theories, boundary value problem, direct model, fragmentation, lattice curvature, aluminum

1. INTRODUCTION

Over several decades there has been sustained interest in the experimental investigation of the behavior of metal and alloy single crystals under various thermal and mechanical loads [1–6]. A single crystal is an object with a relatively simple internal structure, due to which the main (primarily dislocation) mechanisms of inelastic deformation can be analyzed in detail. Along with experimental studies, extensive theoretical research has been conducted in the last 15–20 years based on the use of multilevel crystal plasticity models of single crystal deformation [7–17]. These models reveal the inelastic deformation processes and mechanisms that are not observed experimentally, especially in the bulk of the studied samples. The combined efforts of the physics and mechanics community seeking to develop physically sound theories lead to better single crystal behavior models and to better experimental research methods. As a result, the models describing the inelastic deformation of single crystals can be refined and supplemented, as well as a more accurate description of polycrystalline behavior can be obtained. In the last 10–15 years, some industries (primarily aircraft engine manufacturing) have been actively pursuing the development of single crystal parts and structures, so theoretical and experimental methods for analyzing the behavior of single crystals under various thermal and mechanical loads are also needed to study the manufacture and operation of real single crystal structures.

It is known that the behavior of deformed single crystals as well as their defect structure evolution strongly depends on the mutual orientation of the characteristic loading axes and lattice axes, which is due to the motion of edge dislocations on different sets of slip systems at different orientations. The total number of such systems depends on the type of crystallite (e.g., 12 slip systems for fcc crystals, 48 for bcc) and is completely determined by its crystallography [18, 19]. As a result of slip on different sets of slip systems, the evolution of the stress state and defect structure in a single crystal differs significantly.

Experimental investigation of loaded single crystals revealed a number of general features. Shear deformation behavior strongly depends on the crystallite orientation with respect to the compression axis [1, 20–22]. Single crystals have the tendency to shear localization [20, 23–25]. Studies on the fragmentation of compressed fcc single crystals revealed the formation of specific

zones with different sets of active slip systems within an initially homogeneous single crystal [24]. The location and configuration of these zones substantially depend on the boundary conditions, such as the position and orientation (relative to the characteristic loading directions) of the free and contact surfaces of the single crystal, the conditions on the contact surfaces of the crystal and the die, the mutual orientation of the single crystal faces and crystallographic slip systems.

Since the boundary (and especially contact) conditions have a strong influence of the inhomogeneous deformation behavior, the larger part of Sect. 5 is devoted to their formulation. Contact boundary conditions are formulated as mixed, i.e., kinematic for the normal component and force for the tangential components. In so doing, we specify that the contact surface particles may adhere to the die plate, the contact may break, and slip may occur (Siebel–Amonton–Coulomb law). However, it was not our goal to specially investigate the influence of contact conditions on single crystal behavior; this task is a subject of a separate study.

The mutual orientations of slip systems and free faces largely determine the magnitude and distribution of plastic shear deformation within the crystal. In experiments, initially straight traces of edge dislocations on the surface are curved and the {111} octahedral planes rotate with increasing strain. All cited works show that shear strains and hence the stress-strain state are highly inhomogeneous in single crystals under plastic deformation.

It is known that plastic deformation of crystals occurs mainly by dislocation glide on close-packed planes, wherein moving edge dislocations make the main contribution to inelastic deformation [18, 19, 26–28]. Therefore, the fragmentation of the single crystal volume is essentially determined by the crystal geometry of the deformed sample and by the boundary conditions. Here the single crystal geometry is used to mean a set of geometrical parameters that describe the mutual orientations of the loading axis/axes, lateral faces, and slip systems. Different mutual orientations of the loading axes and lattice axes correspond to slipping on different sets of systems.

As noted above, plastic shearing, dislocation substructures, stresses, and misorientations of some crystal regions relative to others are inhomogeneous in deformed single crystals. At strains of about 3% and higher, initially homogeneous single crystals are fragmented into regions whose internal structure evolves by different scenarios. The task is to understand how the local regions with different internal structure emerge and evolve under inelastic deformation for different orientations of loading axes, lattice axes, and single crystal faces. This paper pays special attention to describing the misorientation of individual single crystal regions under uniaxial compression. We will consider the problem of isolating quasi-rigid body motion from the overall motion, which is of great importance in solving geometrically nonlinear problems [29, 30].

Currently, the behavior of single- and polycrystalline metals and alloys is widely described using a hierarchical approach in which the material is considered as a multilevel system with features specific to each level [31–33], down to micro- and nanoscales of description. This class includes models based on crystal plasticity (elastoviscoplasticity) theories, which explicitly account for the motion of dislocations on crystallographic slip systems and for the anisotropy of the elastic and inelastic properties of single crystals. In this paper, the inelastic behavior of individual crystallites is described using an elastviscoplastic model of the given class [34]. The model has several advantages, e.g., there is no ambiguity in the choice of active slip systems (which is inherent in elastoplastic models) and the counting conditions are relatively stable. When constructing constitutive equations to describe the inelastic deformation of single crystals, we should take into account the presence of geometric nonlinearity [33], including the account of crystal lattice rotations during deformation.

2. MODEL FOR CRYSTALLITE DEFORMATION DESCRIPTION

Here we briefly describe the crystallite deformation model based on the crystal elastoviscoplasticity theory [34]. The total strain rate is measured by the relative velocity gradient $\mathbf{z}$ (with respect to the corotational frame associated with the crystallite lattice), which is an asymmetric and frame-indifferent [35] tensor of the second rank [36]:

$$\mathbf{z} \overset{\text{def}}{=} \hat{\nabla}\mathbf{v}_r^{\mathrm{T}} = \hat{\nabla}\mathbf{v}^{\mathrm{T}} - \boldsymbol{\omega}, \qquad (1)$$

where $\hat{\nabla}$ is the Hamilton operator (nabla operator) defined in the current configuration, $\mathbf{v}_r$ is the velocity of motion relative to the coordinate system rotating with an angular velocity determined by the spin tensor $\boldsymbol{\omega}$, $\mathbf{v}$ is the displacement velocity, and $\boldsymbol{\omega}$ is the spin of quasi-rigid rotation of the rigid coordinate system associated with the crystal lattice of the material, which will be defined below. The nonholonomic measure of total strains $\mathbf{e}$ is determined by the corotational integration of the introduced strain rate:

$$\mathbf{e}^{\mathrm{cr}} = \dot{\mathbf{e}} + \mathbf{e}\cdot\boldsymbol{\omega} - \boldsymbol{\omega}\cdot\mathbf{e} = \hat{\nabla}\mathbf{v}^{\mathrm{T}} - \boldsymbol{\omega}, \quad (2)$$

where $(\cdot)^{\mathrm{cr}}$ is the corotational (indifferent) derivative. This measure and its physical meaning are discussed in more detail in Ref. [37].

The introduced strain rate is assumed to be additively decomposed into the elastic and inelastic components:

$$\mathbf{z} = \mathbf{z}^{\mathrm{e}} + \mathbf{z}^{\mathrm{in}}. \quad (3)$$

The given model assumes that at the initial time point there is a sufficient amount of edge dislocations in the bulk of the material which is necessary for the onset of inelastic deformation. The model does not consider the nucleation, motion, and annihilation of individual dislocations; the glide of dislocations is described by introducing shearing on crystallographic slip systems [18, 19]. Each slip system is characterized by the slip plane normal unit vector **n** and by the direction or normalized Burgers vector **b**, which have fixed directions relative to the crystallographic coordinate system throughout the deformation process. At each point in time, the inelastic component of the relative velocity gradient is determined as follows:

$$\mathbf{z}^{\mathrm{in}} = \sum_{k=1}^{K} \dot{\gamma}^{(k)} \mathbf{b}^{(k)} \mathbf{n}^{(k)}, \quad (4)$$

where $\dot{\gamma}^{(k)}$ is the shear rate on the *k*th slip system. The shear rate on the slip system is determined by the viscoplastic relation [38]

$$\dot{\gamma}^{(j)} = \dot{\gamma}_0 \left(\frac{\tau^{(j)}}{\tau_{\mathrm{c}}^{(j)}} \right)^{1/m} \mathrm{H}(\tau^{(j)} - \tau_{\mathrm{c}}^{(j)}), \quad j = \overline{1, K}, \quad (5)$$

where $\tau^{(j)}$, $\tau_{\mathrm{c}}^{(j)}$ are the actual and critical shear stresses on the *j*th slip system, $\dot{\gamma}_0$ is the shear rate on the slip system when the actual shear stress reaches the critical value, *m* is the rate sensitivity parameter of the material, and *K* is the total number of slip systems in the crystal. The critical shear stresses on the *k*th slip system can be found using an evolutionary equation of the form

$$\dot{\tau}_{\mathrm{c}}^{(k)} = \sum_{j=1}^{J} f_{(j)}^{(k)}(\gamma^{(i)}, \dot{\gamma}^{(i)}; \alpha_{(p)}^{(j)}), \quad i, k = \overline{1, N}, \quad (6)$$

where each term is responsible for a particular hardening mechanism. Here we do not consider hardening, i.e., $\tau_{\mathrm{c}}^{(j)} = \mathrm{const}$ for all slip systems. This assumption was made in order to focus on the analysis of the misorientation of local volumes of the original homogeneous single crystal.

The constitutive equation is the anisotropic Hooke's law in the relaxation form in terms of rates:

$$\boldsymbol{\sigma}^{\mathrm{cr}} \equiv \dot{\boldsymbol{\sigma}} + \boldsymbol{\sigma}\cdot\boldsymbol{\omega} - \boldsymbol{\omega}\cdot\boldsymbol{\sigma} = \boldsymbol{\Pi} : (\mathbf{z} - \mathbf{z}^{\mathrm{in}}), \quad (7)$$

where $\boldsymbol{\Pi}$ is the forth-rank tensor of the elastic properties of the crystallite.

3. GEOMETRIC NONLINEARITY

One of the unresolved problems in nonlinear solid mechanics concerning deformation with large displacement gradients is the isolation of quasi-rigid body motion from the overall motion, or the decomposition of motion into strain-induced and quasi-rigid parts. This issue is closely related to the choice of the corotational derivative, which must be introduced into rate-type constitutive equations in order to satisfy the frame indifference principle. The choice of the given derivative is ambiguous, because formally the number of ways of decomposing motion is as large as the cardinality of the continuum. The main difference in the decomposition methods used is the degree of their physical correctness. In particular, crystal plasticity models are constructed using two main motion decomposition approaches. The first approach is based on the polar decomposition of the deformation gradient. The second one is based on decomposing the velocity gradient into symmetric and antisymmetric (vortex) parts. The main disadvantage of these approaches [39] is the absence of relation between the rigid corotational frame responsible for quasi-rigid motion and the crystallographic directions isolated during the entire process which characterize the symmetry properties of the material. In this regard, the discussed models are not physically sound enough for them to be used for the description of crystal lattice rotation. Earlier we also showed [30, 33, 39] that correct constitutive equations for single crystals (i.e., anisotropic materials) can be derived if the quasi-rigid motion is associated with the lattice and the elasticity tensor components in the basis associated with the crystallographic coordinate system remain unchanged when any rigid rotations are imposed. In this work, we use an approach [33, 39] in which the introduced rigid corotational frame responsible for quasi-rigid motion is associated with one crystallographic direction and with the crystallographic plane containing this direction.

Let us consider in more detail the proposed method of motion decomposition. We introduce a Lagrangian crystallographic coordinate system $Oy^1y^2y^3$ with the basis $\{\mathbf{q}_i\}$ rigidly associated with the crystal lattice. The system is assumed to be Cartesian orthogonal in the reference configuration with its axes aligned, e.g., along the [100], [010] and [001] crystallographic directions of an undistorted cubic lattice. During arbitrary motion of the deformed crystal, the trihedron $\{\mathbf{q}_i\}$ will undergo both rotations and distortions, i.e., its orthonormality will be violated. Note that for crystalline metals and alloys the distortions will be small.

Along with the Lagrangian crystallographic coordinate system, we introduce a Cartesian orthogonal logarithmic corotational coordinate system $Ox^1x^2x^3$ with the orthonormal basis k_i, which coincides with the crystallographic coordinate system in the reference configuration and is associated with the crystallographic coordinate system during the entire deformation process. The relation is specified as follows: the Oy^1 and Ox^1 axes are assumed to coincide at each point in time (the vector $\mathbf{k}_1$ is directed along the vector $\mathbf{q}_1$); at each moment of deformation the vector $\mathbf{k}_2$ is located in the Oy^1y^2 plane orthogonally to the vector $\mathbf{k}_1$. Knowing the position of the vectors $\mathbf{k}_1$ and $\mathbf{k}_2$ at each time point, we can easily determine the position of the third basis vector of the corotational frame: $\mathbf{k}_3 = \mathbf{k}_1 \times \mathbf{k}_2$. Since the corotational frame axes are associated with the crystallite in this case, any rigid rotation of the crystallite will be reproduced by the motion of the corotational frame. It is assumed that plastic deformation does not change the lattice orientation; lattice rotations and distortions are determined only by the elastic part $\hat{\nabla}\mathbf{v}^{\mathrm{e}}$ of the velocity gradient. Omitting the calculations, the spin of the corotational frame $\boldsymbol{\omega}$ relative to the fixed background frame will be expressed by the relation:

$$\begin{aligned}\boldsymbol{\omega} = \dot{\mathbf{k}}_i\mathbf{k}_i = &-(\mathbf{k}_2\cdot\hat{\nabla}\mathbf{v}^{\mathrm{e}}\cdot\mathbf{k}_1)\mathbf{k}_1\mathbf{k}_2 - (\mathbf{k}_3\cdot\hat{\nabla}\mathbf{v}^{\mathrm{e}}\cdot\mathbf{k}_1)\mathbf{k}_1\mathbf{k}_3\\ &+(\mathbf{k}_2\cdot\hat{\nabla}\mathbf{v}^{\mathrm{e}}\cdot\mathbf{k}_1)\mathbf{k}_2\mathbf{k}_1 - (\mathbf{k}_3\cdot\hat{\nabla}\mathbf{v}^{\mathrm{e}}\cdot\mathbf{k}_2)\mathbf{k}_2\mathbf{k}_3\\ &+(\mathbf{k}_3\cdot\hat{\nabla}\mathbf{v}^{\mathrm{e}}\cdot\mathbf{k}_1)\mathbf{k}_3\mathbf{k}_1 + (\mathbf{k}_3\cdot\hat{\nabla}\mathbf{v}^{\mathrm{e}}\cdot\mathbf{k}_2)\mathbf{k}_3\mathbf{k}_2. \qquad (8)\end{aligned}$$

The obtained expression allows us to determine the spin tensor of quasi-rigid motion of the crystallite from the known value of the elastic part of the velocity gradient. Within the approach used, the quasi-rigid rotation of the crystal lattice will be determined by the evolution of plastic shearing in the material and by the total velocity gradient.

4. AN ALGORITHM FOR CALCULATING THE LATTICE CURVATURE

The misorientation of single crystal volumes during deformation can be determined by calculating the curvature and torsion of the crystal lattice. At each point of the material lattice, we may use the Lagrangian crystallographic basis $\{\mathbf{q}_i\}$ with coordinates $\{y^i\}$, which was introduced above to determine the lattice spin whose vectors coincide with the selected axes in the crystal. The crystal lattice rotates as a rigid whole and is elastically distorted under arbitrary deformation. Plastic deformation does not cause lattice distortion. In so doing, elastic lattice distortions are small compared to the inelastic strains acting on the single crystal. Therefore, we will neglect the insignificant elastic lattice distortions when measuring the curvature, and take into account only the rotation of the lattice as a rigid whole. Purely rotational motion is described using the rotation model discussed in the previous section, into which we introduce an orthonormal moving frame with coordinates $\{x^i\}$ whose basis vectors $\{\mathbf{k}_i\}$ are rigidly associated with one crystallographic direction and plane. The orientation of the corotational frame relative to the fixed background frame with the basis $\{\mathbf{e}_i\}$ and coordinates $\{X^i\}$ is determined by the orthogonal tensor:

$$\begin{aligned}\mathbf{O} &= \mathbf{k}_i\mathbf{e}_i,\\ O_{mn} &= \mathbf{e}_m\cdot\mathbf{k}_i\mathbf{e}_i\cdot\mathbf{e}_n = \mathbf{e}_m\cdot\mathbf{k}_n\\ &= \mathbf{k}_m\cdot\mathbf{k}_i\mathbf{e}_i\cdot\mathbf{k}_n = \mathbf{e}_m\cdot\mathbf{k}_n. \qquad (9)\end{aligned}$$

In this case, the characteristics of the lattice curvature and torsion will be completely determined by the difference in the orientations of the corotational frame at infinitely close points of the crystal lattice. According to Ref. [40], the curvature tensor is determined by the relation

$$\boldsymbol{\kappa} = -\frac{1}{2}\boldsymbol{\epsilon}:(\mathbf{O}^{\mathrm{T}}\cdot(\mathbf{O}\nabla)), \qquad (10)$$

where $\boldsymbol{\epsilon}$ is a completely skew-symmetric third-rank Levi-Civita tensor. The expression for the components of the lattice curvature tensor in the basis of the fixed background frame reads:

$$\begin{aligned}\boldsymbol{\kappa} &= -\frac{1}{2}\boldsymbol{\epsilon}:\left(\mathbf{O}^{\mathrm{T}}\cdot(\mathbf{O}\nabla)\right)\\ &= -\frac{1}{2}\boldsymbol{\epsilon}:\left(O_{ij}\mathbf{e}_j\mathbf{e}_i\cdot\left(O_{mn}\mathbf{e}_m\mathbf{e}_n\frac{\partial}{\partial X^k}\mathbf{e}_k\right)\right)\\ &= -\frac{1}{2}\boldsymbol{\epsilon}:\left(O_{ij}\frac{\partial O_{in}}{\partial X^k}\mathbf{e}_j\mathbf{e}_n\mathbf{e}_k\right)\\ &= -\frac{1}{2}\epsilon_{pqr}\mathbf{e}_p\mathbf{e}_q\mathbf{e}_r:\left(O_{ij}\frac{\partial O_{in}}{\partial X^k}\mathbf{e}_j\mathbf{e}_n\mathbf{e}_k\right)\\ &= -\frac{1}{2}\epsilon_{pnj}O_{ij}\frac{\partial O_{in}}{\partial X^k}\mathbf{e}_p\mathbf{e}_k,\\ \kappa_{ij} &= -\frac{1}{2}\epsilon_{inq}O_{mq}\frac{\partial O_{mn}}{\partial X^j}.\end{aligned} \qquad (11)$$

Using the independence of the basis vectors of the fixed background frame $\{\mathbf{e}_i\}$ from the coordinates $\{X^i\}$ and Eq. $(9)_2$, we transform the last relation as

$$\kappa_{ij} = -\frac{1}{2}\in_{inq} O_{mq}\frac{\partial O_{mn}}{\partial X^j} = -\frac{1}{2}\in_{inq} O_{mq}\frac{\partial\left(\mathbf{e}_m\cdot\mathbf{k}_n\right)}{\partial X^j}$$
$$= -\frac{1}{2}\in_{inq} O_{mq}\mathbf{e}_m\cdot\frac{\partial\mathbf{k}_n}{\partial X^j} = -\frac{1}{2}\in_{inq}\mathbf{k}_q\cdot\mathbf{e}_m\mathbf{e}_m\cdot\frac{\partial\mathbf{k}_n}{\partial X^j}, \quad (12)$$
$$\kappa_{ij} = -\frac{1}{2}\in_{inq}\mathbf{k}_q\cdot\frac{\partial\mathbf{k}_n}{\partial X^j}.$$

The tensor $\boldsymbol{\kappa}$ at a certain point $\mathbf{r}$ of the crystal lattice describes the curvature and torsion of three material lattice lines $\mathbf{l}_i$, which are constructed as envelopes of tangent lines to the basis vectors $\mathbf{k}_i$ of the corotational frame in the vicinity of the point $\mathbf{r}$. The diagonal components κ_{ij} $(i=j)$ of the curvature tensor characterize the torsion of the curve $\mathbf{l}_i$, i.e., the "gradient" (or more precisely, directional derivative) of the rotation angle of the trihedron of the corotational frame about the $\mathbf{k}_i$ axis along the same axis. The off-diagonal components κ_{ij} characterize the curvature of the curve $\mathbf{l}_i$ in a plane orthogonal to the vector $\mathbf{k}_i$. In other words, the off-diagonal components κ_{ij} $(i\neq j)$ of the tensor $\boldsymbol{\kappa}$ characterize the curvature of the crystallographic axes of the lattice.

In order for the lattice curvature and torsion to be accurately determined, we need a continuous field of the corotational frame orientations associated with the lattice. In real problem solving, however, the corotational frame orientations are known in a finite set of points, and therefore the curvature can be calculated only approximately. The main difficulty in calculating the curvature tensor components is to calculate the gradient components of the orthogonal tensor $\partial O_{mn}/\partial X^j$.

In this work, the boundary value problem is solved using the finite element method. We propose to use, with some shape functions, a finite element interpolation of the orthogonal tensor values within each finite element:

$$O_{ij}(\mathbf{r}) \approx \sum_p \varphi^{(p)}(\mathbf{r}) O_{ij}^{(p)}(\mathbf{r}^{(p)}), \quad (13)$$

where $\varphi^{(k)}$ are the shape functions of a finite element, $O_{ij}^{(p)}$ is the value of the orthogonal tensor components in the pth finite element node, which are determined separately below, $\mathbf{r}$ is the radius vector lying within the finite element, and $\mathbf{r}^{(p)}$ is the radius vector of the pth finite element node. Then the value of the gradient components O_{ij} within the finite element is calculated as follows:

$$\frac{\partial O_{mn}}{\partial X^j}(\mathbf{r}) \approx \frac{\partial}{\partial X^j}\sum_k \varphi^{(k)}(\mathbf{r}) O_{mn}^{(k)}(\mathbf{r}^{(k)})$$
$$= \sum_k O_{mn}^{(k)}\frac{\partial\varphi^{(k)}(\mathbf{r})}{\partial X^j}. \quad (14)$$

Thus, the value of the components of the curvature tensor $\boldsymbol{\kappa}$ within the finite element is completely determined by the value of the orthogonal tensor components in the finite element nodes and by the shape functions of the given finite element:

$$\kappa_{ij}(\mathbf{r}) \approx -\frac{1}{2}\in_{inq} O_{mq}(\mathbf{r})\left(\sum_k O_{mn}^{(k)}\frac{\partial\varphi^{(k)}(\mathbf{r})}{\partial X^j}\right), \quad (15)$$
$$\kappa_{ij}(\mathbf{r}) \approx -\frac{1}{2}\in_{inq}\left(\sum_p \varphi^{(p)}(\mathbf{r}) O_{mq}^{(p)}\right)$$
$$\times\left(\sum_k O_{mn}^{(k)}\frac{\partial\varphi^{(k)}(\mathbf{r})}{\partial X^j}\right),$$

where Eqs. (11)–(14) are used, and $\mathbf{r}$ belongs to the finite element space.

It should be noted that, in the case of using the finite element method, the velocity of the lattice-associated corotational frame (determined by model (8)) is calculated at integration points that are rigidly associated with the material (i.e., have constant Lagrangian coordinates) and lie within the finite element. When dealing with orientations of three-dimensional objects, it is convenient to use quaternions, whose components are one-to-one related with the orthogonal tensor components [41]. A quaternion has four components, which are expressed through the angle of rotation φ and vector $\mathbf{u}$ directed along the axis of rotation:

$$\mathrm{q}_i = \left\{\cos\frac{\varphi}{2}, \sin\frac{\varphi}{2}\mathrm{u}_1, \sin\frac{\varphi}{2}\mathrm{u}_2, \sin\frac{\varphi}{2}\mathrm{u}_3\right\},$$
$$\mathbf{q} = \left\{\cos\frac{\varphi}{2}, \sin\frac{\varphi}{2}\mathbf{u}\right\}. \quad (16)$$

During solution, the component values of the quaternion $\mathbf{q}$ are calculated only at integration points, after which (at each solution step) the quaternion component values are calculated separately at finite element nodes by averaging over the final elements adjacent to the node in the following way. For each node N, we calculate an array of integration points $\mathbf{I}_k$ of those finite elements to which the considered node belongs. Then, weighting factors $\mathbf{w}_k$ are determined for these integration points as follows:

$$w_k = \frac{\mathrm{s}^{-1}}{l_k}, \quad s = \sum_i \frac{1}{l_i},$$

where l_k is the distance from the considered node to the kth integration point $k\in I_k$. After that, the mean lattice orientation value is calculated by the weighting factors and the values at the adjacent integration points:

$$\mathbf{q}_N = \sum_k w_k\mathbf{q}_k, \quad (17)$$

where $\mathbf{q}_N, \mathbf{q}_k$ are the quaternions defining the orientation in the node with number N and at the adjacent inte-

gration points, respectively. Equation (17) is a generalization of linear interpolation between two orientations [41]. To assess the accuracy of this method for obtaining the nodal values of the corotational frame orientation, we calculated the mismatch angle δ between the orientation q_I at the integration point with number *I*, which is obtained directly from the material model, and the orientation at the integration point $\tilde{q}_I$, found by interpolation of the nodal values:

$$\tilde{\mathbf{q}}_I = \sum_N \varphi^{(N)}(\mathbf{r}_I)\,\mathbf{q}_N, \tag{18}$$

where $\mathbf{q}_N$ is the quaternion that defines the orientation in the node with number *N* belonging to the finite element with integration point *I*, which is calculated by Eq. (17), and $\mathbf{r}_I$ is the radius vector of the position of the integration point with number *I*. It is known that the sequence of two rotations specified by the quaternions $\mathbf{q}_1$, $\mathbf{q}_2$ determines the rotation $\mathbf{q} = \mathbf{q}_2 \circ \mathbf{q}_1$, where $\circ$ is the quaternion multiplication, the result of which is also a quaternion. In our case, we may introduce the quaternion $\mathbf{q}_\delta$ that matches the orientations $\tilde{\mathbf{q}}_I$ and $\mathbf{q}_I$: $\mathbf{q}_I = \mathbf{q}_\delta \circ \tilde{\mathbf{q}}_I$. Hence the angle δ by which the quaternion $\mathbf{q}_\delta$ (16) specifies the rotation is the desired discrepancy. In the numerical experiment, we determined the quantity

$$\Delta = \max_{i,\varphi_i > 0.001} (\delta_i / \varphi_i),$$

where *i* is the number of the integration point, and φ_i is the angle of rotation of the lattice-associated corotational frame at the integration point *i*. In so doing, the maximum was computed in all integration points where the corotational frame rotation was not less than 10^{-3} rad. As a result, the value of Δ was found not to exceed 15%.

5. DIRECT MODEL. APPLICATION OF FINITE ELEMENT METHOD

This section will consider the problem of uniaxial compression of an Al single crystal with orientation D1 [24] (Fig. 1). The lateral faces coincide with the (001) and $(\bar{1}10)$ crystallographic planes, and the compression axis coincides with the (110) crystallographic direction. The commercial purity aluminum single crystal with the dimensions 6 × 3 × 3 mm is confined between two punches P_1 and P_2. There is friction between the punches and the sample. The upper punch moves progressively with the velocity $\mathbf{v} = \{0, 0, -V\}$; the lower punch is fixed.

At the time point *t*, the single crystal body occupies the region Ω^t with the boundary S^t. It is necessary to determine the fields of velocities **v** and stresses $\boldsymbol{\sigma}$ at any time point which would satisfy the (rate-type) equilibrium equation [29]:

$$\hat{\nabla} \cdot \dot{\boldsymbol{\sigma}} - \hat{\nabla} \cdot (\mathbf{v} \cdot \hat{\nabla} \boldsymbol{\sigma}) = \mathbf{0}, \quad \mathbf{r} \in \Omega^t, \tag{19}$$

$\hat{\nabla}$ is the nabla-operator in the current configuration, and the constitutive equations of the material model (1)–(8). The single crystal boundary is represented in the general case as

$$S^t = S^{\text{free}}(t) \cup S^{\text{cont}}(t), \tag{20}$$

$S^{\text{free}}(t)$ is the free boundary, and $S^{\text{cont}}(t)$ is the contact boundary (mixed boundary conditions: force and kinematic). The faces *ABCD* and $A_1B_1C_1D_1$ are the areas of possible contact where the mixed boundary conditions are specified. The contact boundary $S^{\text{cont}}(t)$ is a priori unknown. We determine it using the approach described in detail in Ref. [29], for which the contact boundary is divided into three zones: adhesion zone S^*_{ca}, detachment zone S^*_{cd}, and slip zone S^*_{cs}.

Below is the complete set of boundary conditions for the considered boundary value problem of single crystal deformation; all components are defined in the basis of the fixed background frame:

1) the upper punch performs a translational rectilinear motion with a given constant velocity, the lower punch is rigidly fixed:

$$\begin{cases} \mathbf{v}|_{P_1} = \{0, 0, -V\}, \\ \mathbf{v}|_{P_2} = \{0, 0, 0\}, \end{cases}$$

2) the lateral faces are under trivial static boundary conditions (also rate-type ones) [29]:

$$\mathbf{n} \cdot \dot{\boldsymbol{\sigma}} + (\mathbf{n} \cdot \hat{\nabla} \mathbf{v} \cdot \mathbf{n}) \mathbf{n} \cdot \boldsymbol{\sigma} - (\hat{\nabla} \mathbf{v} \cdot \mathbf{n}) \cdot \boldsymbol{\sigma} = \mathbf{0},$$
$$\mathbf{r} \in S_3 \cup S_4 \cup S_5 \cup S_6;$$

3) contact conditions: the end faces are under the mechanical contact condition; friction is determined by the

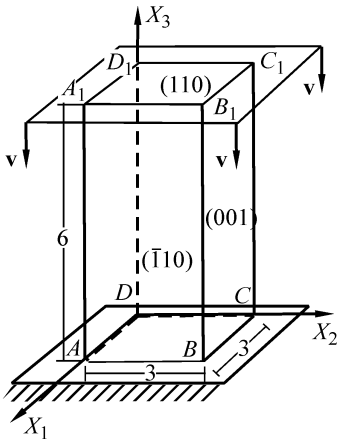

Fig. 1. Schematic computational domain of a single crystal with orientation D1 (dimensions are indicated in mm) and the coordinate axes of the fixed background frame, P_1, P_2 are the upper and lower punches, $S_1 = A_1B_1C_1D_1$, $S_2 = ABCD$, S_{3-6} are the lateral faces.

Siebel–Amonton–Coulomb law. The velocity of the punch points will be denoted by $\mathbf{v}^{\mathrm{p}}$, and that of the single crystal surface will be $\mathbf{v}^{\mathrm{m}}$. The surface areas of the geometric contact can be in three states: adhesion zone, where the velocities of contacting surface points are

$$\mathbf{v}^{\mathrm{p}}(\mathbf{r},t) = \mathbf{v}^{\mathrm{m}}(\mathbf{r},t), \quad \mathbf{r}\in S^{*}_{\mathrm{ca}},$$

detachment zone, or the surface area that was previously in contact and has turned to the free surface by the current time point, is determined by the conditions $\sigma_{\mathrm{nn}}=0$, $\dot{\sigma}_{\mathrm{nn}}\geq 0$:

$$\dot{\boldsymbol{\sigma}}_{\mathrm{n}}(\mathbf{r},t)=\mathbf{0}, \quad \mathbf{r}\in S^{*}_{\mathrm{cd}},$$

slip zone:

$$\mathrm{v}^{\mathrm{p}}_{\mathrm{n}}(\mathbf{r},t) = \mathrm{v}^{\mathrm{m}}_{\mathrm{n}}(\mathbf{r},t),$$

$$\dot{\boldsymbol{\sigma}}_{\tau}(\mathbf{r},t)=-\dot{\tau}_{f}\frac{\mathbf{v}^{\mathrm{p}}_{\tau}(\mathbf{r},t)-\mathbf{v}^{\mathrm{m}}_{\tau}(\mathbf{r},t)}{|\mathbf{v}^{\mathrm{p}}_{\tau}(\mathbf{r},t)-\mathbf{v}^{\mathrm{m}}_{\tau}(\mathbf{r},t)|}, \quad \mathbf{r}\in S^{*}_{\mathrm{cs}},$$

$$\dot{\tau}_{f}=\begin{cases} f\,\dot{\sigma}_{\mathrm{n}} \text{ at } \mu\dot{\sigma}_{\mathrm{nn}}<\dot{\tau}_{\mathrm{y}}, \\ \dot{\tau}_{\mathrm{y}} \text{ at } \mu\dot{\sigma}_{\mathrm{nn}}\geq\dot{\tau}_{\mathrm{y}}, \end{cases}$$

where $\boldsymbol{\sigma}_{\mathrm{n}}=\mathbf{n}\cdot\boldsymbol{\sigma}$, $\sigma_{\mathrm{nn}}=\mathbf{n}\cdot\boldsymbol{\sigma}\cdot\mathbf{n}$, $\boldsymbol{\sigma}_{\tau}=\boldsymbol{\sigma}_{\mathrm{n}}-\sigma_{\mathrm{nn}}\mathbf{n}$ are the stress vector on the surface area with normal $\mathbf{n}$, its normal and tangential components, $\mathbf{v}^{\mathrm{m}}_{\mathrm{n}}$, $\mathbf{v}^{\mathrm{m}}_{\tau}$ are the normal and surface tangential components of the velocity of the single crystal points, $\mathbf{v}^{\mathrm{p}}_{\mathrm{n}}$, $\mathbf{v}^{\mathrm{p}}_{\tau}$ are the normal and surface tangential components of the velocity of the punch points, $\dot{\tau}_{\mathrm{y}}$ is the rate of change in the yield strength of the material at the contact point, and μ is the friction coefficient;

4) initial conditions:

$$\begin{aligned} &\mathbf{u}=\mathbf{0}: \quad \mathbf{r}\in\Omega^{0}, \\ &\boldsymbol{\sigma}=\mathbf{0}, \quad \mathbf{r}\in\Omega^{0}; \end{aligned} \tag{21}$$

5) displacements $\mathbf{u}$ and stresses $\boldsymbol{\sigma}$ for a material particle are determined by integration (taking into account the known Lagrangian motion equation $\mathbf{r}=\mathbf{r}(\xi^{i},t)$):

$$\begin{aligned} &\mathbf{u}(\xi^{i},t)=\int_{0}^{t}\mathbf{v}(\mathbf{r}(\xi^{i},\tau),\tau)\mathrm{d}\tau, \quad \{\xi^{i}\}\in\mathcal{B}(0), \\ &\boldsymbol{\sigma}(\xi^{i},t)=\boldsymbol{\sigma}_{0}(\xi^{i})+\int_{0}^{t}\dot{\boldsymbol{\sigma}}(\mathbf{r}(\xi^{i},\tau),\tau)\mathrm{d}\tau, \quad \{\xi^{i}\}\in\mathcal{B}(0), \end{aligned} \tag{22}$$

where $\mathcal{B}$ is the area occupied by the single crystal material.

The formulated problem was solved using a direct model of the first type [42] based on the finite element method. In the model, the described object is a separate single crystal (in the initial state) approximated by a set of finite elements. Here we used four-node simplex elements with one integration point; in this case, each finite element is a crystallite. The response of the given crystallite is determined using crystal elastoviscoplasticity theory (1)–(8). The displacement velocities of each nodal point are calculated when solving the boundary value problem; the velocity values are used to calculate the velocity gradients, which are the kinematic input data for the discussed crystallite model.

A four-node simplex element implies an approximation using four linear functions of the form

$$\varphi^{(k)}(x^{1},x^{2},x^{3})=\alpha_{0}^{(k)}+\alpha_{1}^{(k)}x^{1}+\alpha_{2}^{(k)}x^{2}+\alpha_{3}^{(k)}x^{3}, \tag{23}$$

any field of values of a quantity A is interpolated within a finite element as follows:

$$\tilde{A}(x^{1},x^{2},x^{3},t)=A^{(k)}(t)\varphi^{(k)}(x^{1},x^{2},x^{3}), \tag{24}$$

where $A^{(k)}$ is the value of the quantity A in the node k.

The total number of simplex elements into which the computational domain (single crystal volume) was divided was about 164 000; the total number of degrees of freedom of the solved problem was about 32 000. The punches were modeled by flat rigid plates; the surface of each plate was approximated by 150 triangular finite elements.

The finite element solution of the formulated boundary value problem was computed using original software. The ANSYS 18 package was applied to model the computational domain, to construct the grid, and to determine the boundary conditions. The results were visualized using the free ParaView 5.2.0 software.

6. EVALUATION OF SINGLE CRYSTAL VOLUME FRAGMENTATION

The main goal of this work was to study the fragmentation of the original homogeneous single crystal into volumes that differ in the evolution of inelastic deformation and have different crystal lattice orientation.

Figure 2 shows the intensity distribution of the plastic strain rate in single crystal regions located in the vicinity of the face $CDD_{1}C_{1}$ at a relative strain of 0.2–0.35%. The presented results show that plastic deformations first appear in the volumes adjacent to the edges of the sample faces contacting with the punches and then propagate into the crystal bulk. The initiation of plastic shearing was investigated in detail in our earlier paper [43] that focused on the processes occurring beyond a strain of 1%. There we used the finite element software ABAQUS with the user defined material subroutine UMAT. The use of UMAT had some disadvantages because it was impossible to correctly describe geometric nonlinearity, and the computation was much more time

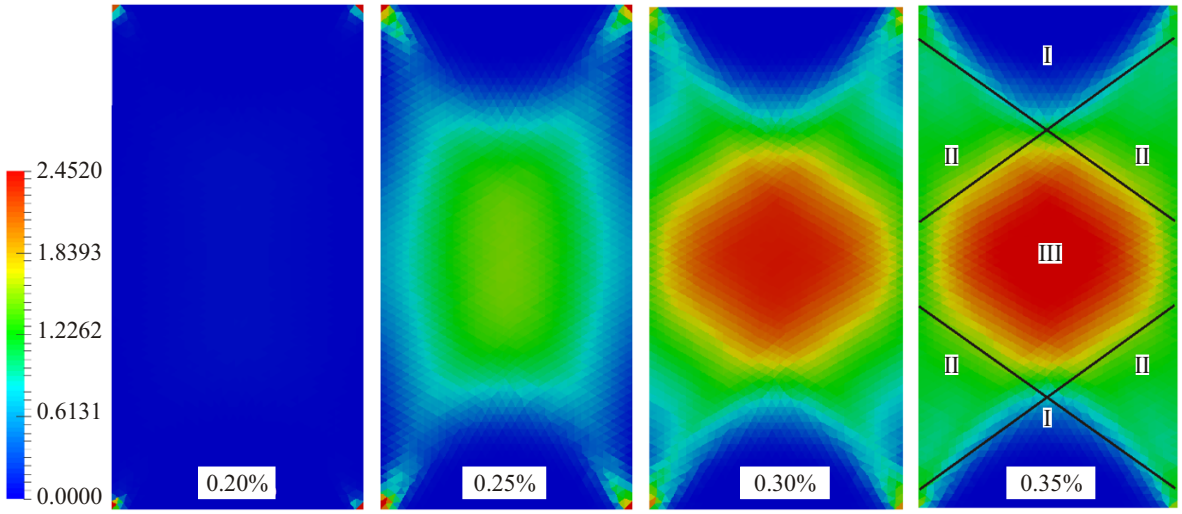

Fig. 2. Plastic strain rate intensity distribution in the single crystal region adjacent to the face CDD_1C_1 at a relative strain of 0.20–0.35% (color online).

consuming than when using our original software package. Due to the presence of anisotropy and inhomogeneous deformation, the single crystal is fragmented into 7 volumes (of three types) with different plastic strain intensity, which was also predicted theoretically and observed in a full-scale experiment [24]. As was shown in Ref. [43], different sets of slip systems are active in these volumes. The regions adjacent to the boundaries of these volumes have the largest gradients of plastic strain intensity and the largest differences in lattice rotations.

The distribution and value of the plastic strain rate intensity changes insignificantly during single crystal compression, as illustrated in Fig. 3. Note that the shape of the fragments obtained with the use of ABAQUS/UMAT was different, e.g., the central fragment had a shape close to a regular hexagon. The original single crystal is fragmented into volumes with different inelastic strain intensity, which persists throughout the process (up to a 6% relative strain). Due to the presence of large shear strains in zone III, the material moves mainly along the [001] direction [43], while the motion of the material in zones I near the end faces is hindered due to large friction forces. This way of material deformation leads to large rotations in zones II.

According to the results depicted in Fig. 4, the maximum absolute value of the angle of crystal lattice rota-

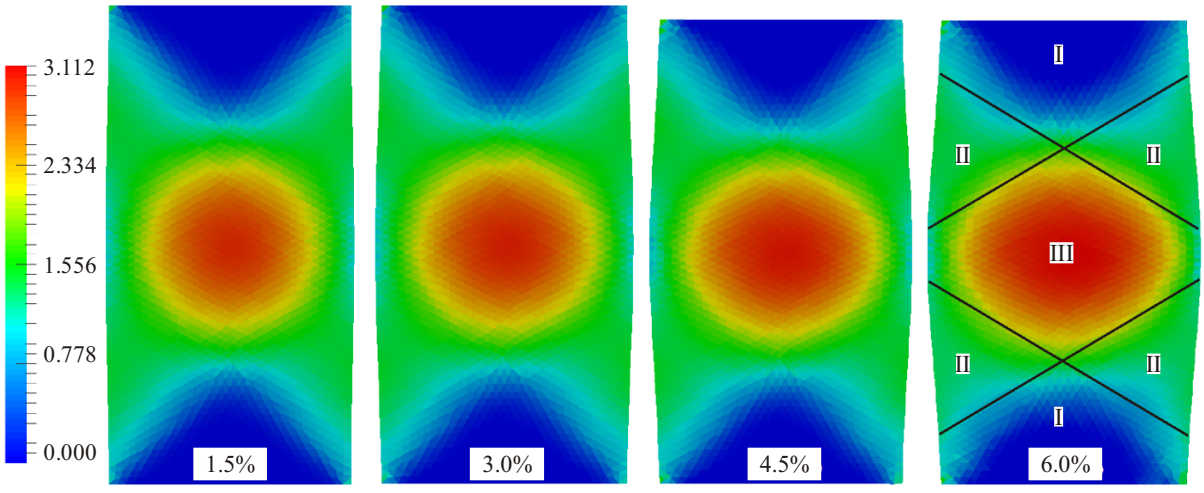

Fig. 3. Plastic strain rate intensity distribution in the single crystal region adjacent to the face CDD_1C_1 at a relative strain of 1.5–6.0% (color online).

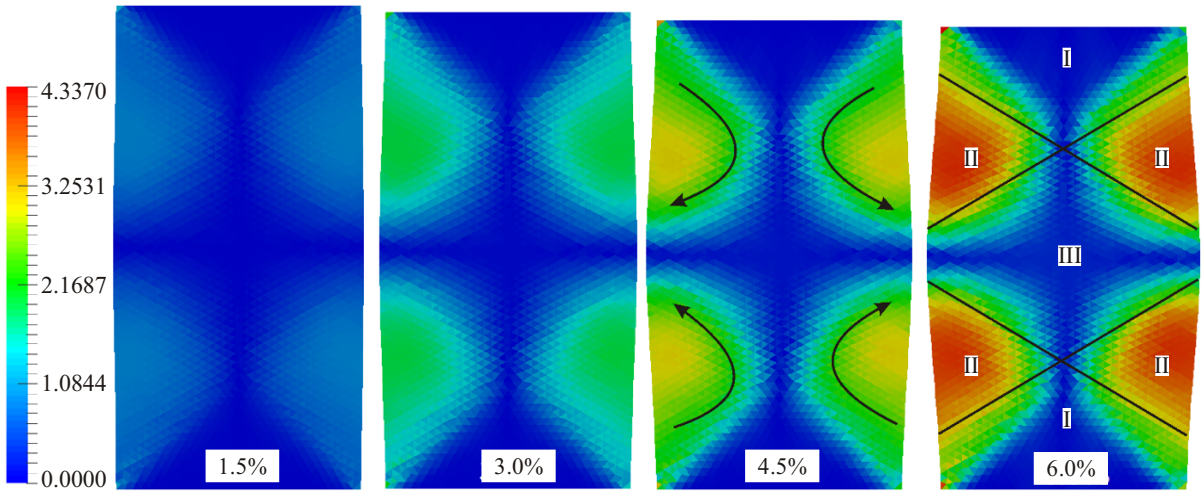

Fig. 4. Distribution of the absolute value of the angle of lattice rotation (degrees) in material points about the X_1 axis of the fixed background frame on the face CDD_1C_1 at a relative strain of 1.5–6.0%; the arrows indicate the direction of lattice rotation (color online).

tion about the $[\bar{1}10]$ axis (perpendicular to the figure plane) is achieved in volumes II, while the minimum one is achieved in zones I and III. Previous experiments [44] revealed that traces of shear along the (111), $(11\bar{1})$ planes in zones II (on the CDC_1D_1 surface) make up an angle of about 3° with the same planes in the undeformed state. The inhomogeneous rotation of the crystal lattice leads to its curvature.

Figure 5 shows the distribution of the norm of the curvature tensor $\sqrt{\boldsymbol{\kappa}:\boldsymbol{\kappa}^{\mathrm{T}}}$ (15) for the relative strains 1.5–6.0%. These results indicate that the initially homogeneous single crystal is divided into misoriented fragments with a well-defined boundary. The boundary thickness does not exceed 0.3 mm (the height of the original sample is 6 mm). The relative position of the fragments remains unchanged during deformation up to a 6% relative strain.

The next figure (Fig. 6) shows the distribution of the component κ_{21} of the curvature tensor $\boldsymbol{\kappa}$ (for the relative strain 1.5–6.0%) which characterizes the curvature of the material lattice line $\mathbf{l}_2$ (the envelope of tangent lines to the corotational frame vector $\mathbf{k}_2$) in the plane orthogonal to the corotational frame vector $\mathbf{k}_1$. The maximum deviation of the corotational frame vector $\mathbf{k}_1$ from the vector of the fixed background frame $\mathbf{e}_1$ does not exceed 0.5° in zones *K*, and hence the plane orthogonal to $\mathbf{k}_1$ almost coincides with the plane X_2X_3 of the fixed background frame. The maximum absolute value of the

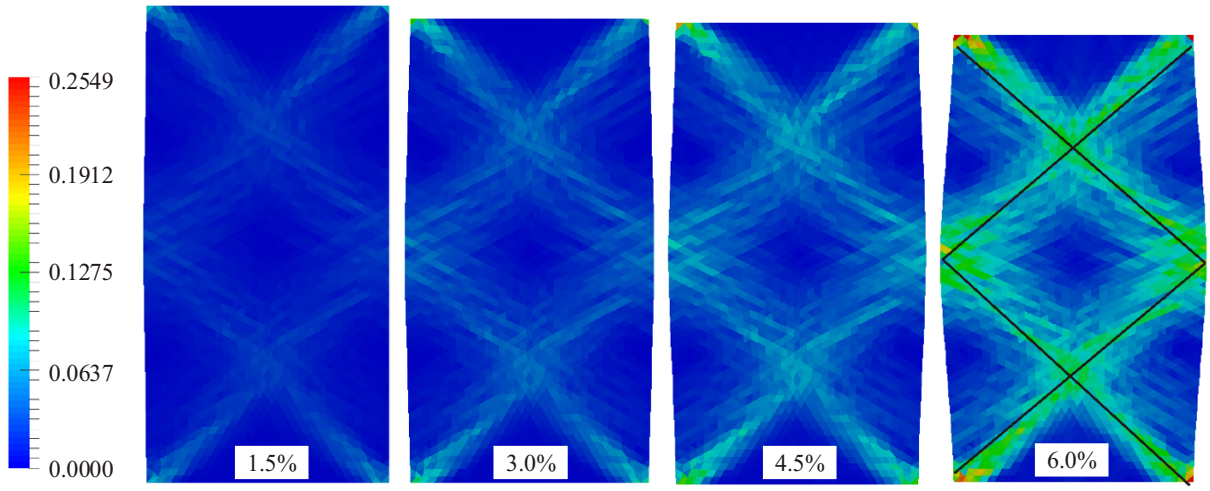

Fig. 5. Distribution of the norm of the lattice curvature tensor in the near-surface layer of the face CDD_1C_1 at a relative strain of 1.5–6.0% (color online).

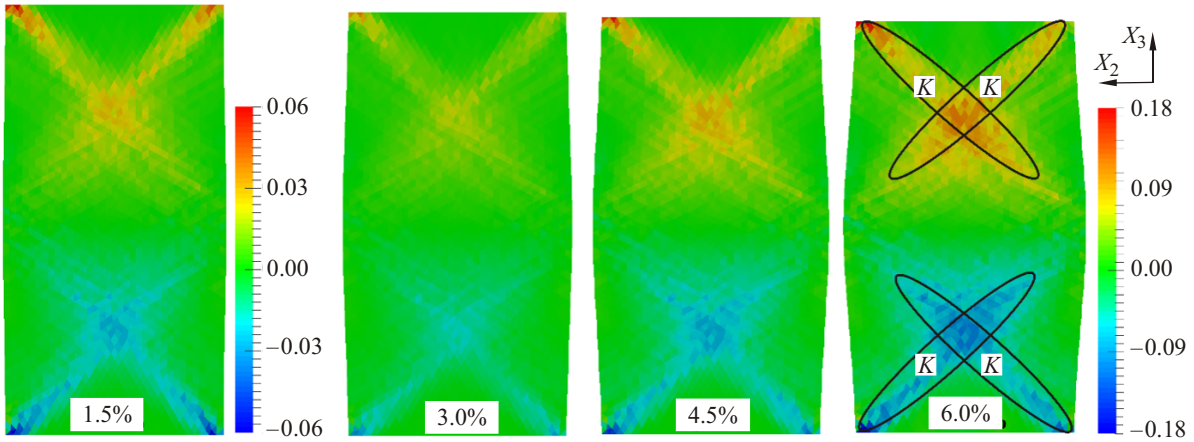

Fig. 6. Distribution of the lattice curvature component 21 on the face CDD_1C_1 of the single crystal at a relative strain of 1.5–6.0%; the ellipses denote the zones with the maximum absolute value (color online).

curvature is achieved in zones *K* (Fig. 6). In a full-scale experiment, these zones exhibit curved traces (lying in the plane X_2X_3) of edge dislocations that produce shear on the (111), $(11\bar{1})$ planes (Fig. 7), which is an indirect indicator of the crystal lattice curvature.

It should be noted that there is a close symbiotic relationship between inhomogeneous plastic shearing and lattice rotations/torsions, which was discussed in the works by Panin and colleagues (see, e.g., [45]). Indeed, lattice rotations are substantially determined by plastic shearing on slip systems. The higher is the plastic shear inhomogeneity, the greater is the difference in lattice rotations, and therefore the higher are the absolute values of the components and norms of the torsion-curvature tensor. This statement is fully consistent with the theoretical results obtained. By comparing the results illustrated in Figs. 2, 3 and 5, it is easy to see that the regions with the largest curvature/torsion coincide with the zones of the highest plastic strain gradients.

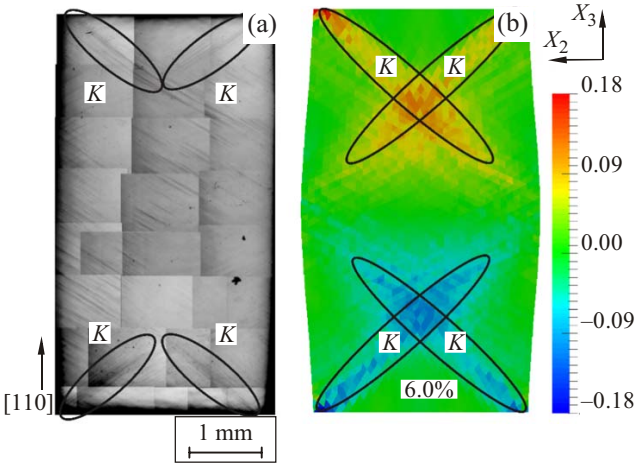

Fig. 7. Experimentally observed surface of the face CDD_1C_1 of the single crystal (a) and the distribution of the curvature component κ_{21} on the same face at a relative strain of 6.0% (b) (color online).

7. CONCLUSIONS

This study modeled the uniaxial compression of a single crystal sample. The formulated problem was solved using a first-type direct model based on the finite element method. The response of the material was determined by a crystal elastoviscoplasticity model that explicitly takes into account shearing on real crystallographic planes. The modeling results showed that the original homogeneous volume of the single crystal is divided into 7 fragments during deformation, in which the shear strain intensity differs by several orders of magnitude; the maximum intensity value is reached in the central region of the sample, while the minimum one is observed in the regions near the end faces. Inhomogeneous plastic shearing causes a misorientation of the formed fragments; the maximum misorientation of neighboring fragments reaches 8°, and the crystal lattice rotation in them relative to the undeformed state reaches 4° at a relative strain of 6%. As a result of inhomogeneous lattice rotation, the lattice in some regions of the single crystal (between the fragments) is curved. The numerical experiment showed that the single crystal lattice is curved in some regions during compression, which agrees with the results of the full-scale experiment where

curved slip traces of edge dislocations were also observed on the surface.

FUNDING

The work was carried out at the support of the RSF Grant No. 17-19-01292.

REFERENCES

1. Teplyakova, L.A., Kunitsyna, T.S., and Koneva, N.A., Orientation Effect of L12 Superlattice Ni_3Fe Alloy Monocrystals on Substructure Formation under Compression, *Deform. Razrush. Mater.*, 2015, no. 2, pp. 40–48.
2. Teplyakova, L.A., Bespalova, I.V., and Lychagin, D.V., Spatial Organization of Deformation in Aluminum [1–12] Single Crystals in Compression, *Phys. Mesomech.*, 2009, vol. 12, no. 3–4, pp. 166–174.
3. Lychagin, D.V., Tarasov, S.Yu., Chumaevskii, A.V., and Alfyorova, E.A., Macrosegmentation and Strain Hardening Stages in Copper Single Crystals under Compression, *Int. J. Plasticity*, 2015, vol. 69, pp. 36–53.
4. Saai, A., Louche, H., Tabourot, L., and Chang, H.J., Experimental and Numerical Study of the Thermo-Mechanical Behavior of Al Bi-Crystal in Tension Using Full Field Measurements and Micromechanical Modeling, *Mech. Mater.*, 2010, vol. 42, pp. 275–292.
5. Groh, S., Marin, E.B., Horstemeyer, M.F., and Zbib, H.M., Multiscale Modeling of the Plasticity in an Aluminum Single Crystal, *Int. J. Plasticity*, 2009, vol. 25, pp. 1456–1473.
6. Dumoulin, S. and Tabourot, L., Experimental Data on Aluminium Single Crystal Behaviour, *Proc. Inst. Mech. Eng. C*, 2005, vol. 219, no. 9, pp. 1159–1167.
7. Liu, M., Lu, C., and Tieu, A.K., Crystal Plasticity Finite Element Method Modelling of Indentation Size Effect, *Int. J. Solid. Struct.*, 2015, vol. 54, pp. 42–49.
8. Gerard, C., Cailletaud, G., and Bacroix, B., Modeling of Latent Hardening Produced by Complex Loading Paths in FCC Alloys, *Int. J. Plasticity*, 2013, vol. 42, pp. 194–212.
9. Wang, Z.Q., Beyerlein, I.J., and LeSar, R., Plastic Anisotropy in FCC Single Crystal in High Rate Deformation, *Int. J. Plasticity*, 2009, vol. 25, pp. 26–48.
10. Preussner, J., Rudnik, Y., Brehm, H., Volkl, R., and Glatzel, U., A Dislocation Density Based Material Model to Simulate the Anisotropic Creep Behavior of Single-Phase and Two-Phase Single Crystals, *Int. J. Plasticity*, 2009, vol. 25, no. 5, pp. 973–994. doi 10.1016/j.ijplas.2008.04.006
11. Ha, S., Jang, J.-H., and Kim, K.T., Finite Element Implementation of Dislocation-Density-Based Crystal Plasticity Model and Its Application to Pure Aluminum Crystalline Materials, *Int. J. Mech. Sci.*, 2017, vol. 120, pp. 249–262. doi 10.1016/j.ijmecsci.2016.11.011
12. Harder, J., FEM-Simulation of the Hardening Behavior of FCC Single Crystals, *Acta Mech.*, 2001, vol. 150, pp. 197–217.
13. Horstemeyer, M.F., Potirniche, G.P., and Marin, E.B., Crystal Plasticity, in *Handbook of Materials Modeling*, Yip, S., Ed., Netherlands: Springer, 2005, pp. 1133–1149.
14. Roters, F., Application of Crystal Plasticity FEM from Single Crystal to Bulk Polycrystal, *Comput. Mater. Sci.*, 2005, vol. 32, pp. 509–517.
15. Staroselsky, A. and Anand, L., A Constitutive Model for HCP Materials Deforming by Slip and Twinning: Application to Magnesium Alloy AZ31B, *Int. J. Plasticity*, 2003, vol. 19, pp. 1843–1864.
16. Wang, H., Wu, P.D., Wang, J., and Tome, C.N., A Crystal Plasticity Model for Hexagonal Close Packed (HCP) Crystals Including Twinning and De-Twinning Mechanisms, *Int. J. Plasticity*, 2013, vol. 49, pp. 36–52. doi 10.1016/j.ijplas.2013.02.016
17. Zaafarani, N., Raabe, D., Singh, R.N., Roters, F., and Zaefferer, S., Three-Dimensional Investigation of the Texture and Microstructure below a Nanoindent in a Cu Single Crystal Using 3D EBSD and Crystal Plasticity Finite Element Simulations, *Acta Mater.*, 2006, vol. 54, pp. 1863–1876.
18. Hirth, J.P. and Lothe, J., *Theory of Dislocations*, New York–St. Louis–San Francisco: McGraw-Hill Book Company, 1970.
19. Honeycombe, R.W.K., *The Plastic Deformation of Metals*, London–Baltimore: E. Arnold, 1984.
20. Asaro, R.J., Geometrical Effects in the Inhomogeneous Deformation of Ductile Single Crystals, *Acta Metall.*, 1979, vol. 27, no. 3, pp. 445–453.
21. Peirce, D., Asaro, R., and Needleman, A., An Analysis of Nonuniform and Localized Deformation in Ductile Single Crystals, *Acta Metall.*, 1982, vol. 30, pp. 1087–1119.
22. Szczerba, M. and Korbel, A., Strain Softening and Instability of Plastic Flow in Cu–Al Single Crystals, *Acta Metall.*, 1987, vol. 35, no. 5, pp. 1129–1135.
23. Teplyakova, L.A., Lychagin, D.V., and Kozlov, E.V., Shear Localization in Deformed Al Single Crystals with a Compression Axis Orientation [001], *Phys. Mesomech.*, 2003, vol. 6, no. 1–2, pp. 19–24.
24. Teplyakova, L.A., Lychagin, D.V., and Bespalova, I.V., Mechanisms of Deformation Macrolocalization in Aluminium Single Crystals with Loading Axis Orientation [110], *Fiz. Mezomekh.*, 2004, vol. 7, no. 6, pp. 63–78.
25. Chang, Y.W. and Asaro, R.J., An Experimental Study of Shear Localization in Aluminum-Copper Single Crystals, *Acta Metall.*, 1981, vol. 29, no. 1, pp. 241–257.
26. Friedel, J., *Les Dislocations*, Paris: Gauthiers–Villar, 1956.
27. Mirkin, L.I., *Physical Foundations of Strength and Plasticity: Introduction into Theory of Dislocations*, Moscow: MGU, 1968.
28. Novikov, I.I., *Crystal Structure Defects in Metals: A Textbook*, Moscow: Metallurgiya, 1975.

29. Pozdeev, A.A., Trusov, P.V., and Nyashin, Yu.I., *Large Elastoplastic Deformations: Theory, Algorithms, Applications*, Moscow: Nauka, 1986.
30. Trusov, P.V., Shveykin, A.I., and Yanz, A.Yu., Motion Decomposition, Frame-Indifferent Derivatives, and Constitutive Relations at Large Displacement Gradients from the Viewpoint of Multilevel Modeling, *Phys. Mesomech.*, 2017, vol. 20, no. 4, pp. 357–376.
31. Panin, V.E., Egorushkin, V.E., and Panin, A.V., Physical Mesomechanics of a Deformed Solid as a Multilevel System. I. Physical Fundamentals of the Multilevel Approach, *Phys. Mesomech.*, 2006, vol. 9, no. 3–4, pp. 9–20.
32. Makarov, P.V., Mathematical Theory of Evolution of Loaded Solids and Media, *Phys. Mesomech.*, 2008, vol. 11, no. 5–6, pp. 213–227.
33. Trusov, P.V. and Shveykin, A.I., On Motion Decomposition and Constitutive Relations in Geometrically Nonlinear Elastoviscoplasticity of Crystallites, *Phys. Mesomech.*, 2017, vol. 20, no. 4, pp. 377–391.
34. Trusov, P.V., Shveykin, A.I., Nechaeva, E.S., and Volegov, P.S., Multilevel Models of Inelastic Deformation of Materials and Their Application for Description of Internal Structure Evolution, *Phys. Mesomech.*, 2012, vol. 15, no. 3–4, pp. 155–175.
35. Truesdell, C., *Rational Thermodynamics; A Course of Lectures on Selected Topics*, New York: McGraw-Hill, 1969.
36. Trusov, P.V., Nechaeva, E.S., and Shveykin, A.I., Asymmetric Stress-Strain Measures in Construction of Multilevel Constitutive Models of Materials, *Fiz. Mezomekh.*, 2013, vol. 16, no. 2, pp. 15–31.
37. Trusov, P.V. and Yanz, A.Yu., Physical Meaning of Nonholonomic Strain Measure, *Phys. Mesomech.*, 2016, vol. 19, no. 2, pp. 215–222.
38. Asaro, R.J. and Needleman, A., Texture Development and Strain Hardening in Rate Dependent Polycrystals, *Acta Metall.*, 1985, vol. 33, no. 6, pp. 923–953.
39. Yanz, A.Yu., *A Two-Level Model for the Description of Inelastic Deformation of Polycrystals: An Application to the Analysis of Multiaxial Loading in the Case of Large Displacement Gradients*, Cand. Degree Thesis (Phys. & Math.), Perm: IMSS UrO RAN, 2016.
40. Pietraszkiewicz, W. and Eremeyev, V.A., On Natural Strain Measures of the Nonlinear Micropolar Continuum, *Int. J. Solid. Struct.*, 2009, vol. 46, no. 3–4, pp. 774–787.
41. Gordeev, V.N., *Application of Quaternions and Biquaternions in Geometry and Mechanics*, Kiev: Stal, 2016.
42. Trusov, P.V. and Shveykin, A.I., Multilevel Crystal Plasticity Models of Single- and Polycrystals. Direct Models, *Phys. Mesomech.*, 2013, vol. 16, no. 2, pp. 99–124.
43. Yants, A.Yu. and Teplyakova, L.A., Modeling of Loading of Single Crystal Samples, *Russ. Phys. J.*, 2015, vol. 58, no. 3, pp. 330–335.
44. Bespalova, I.V., *Effect of Crystal Geometry on Fragmentation and Shear Strain Localization in Aluminum Single Crystals under Compression*, Cand. Degree Thesis (Phys. & Math.), Tomsk: IFPM SO RAN, 2008.
45. Panin, V.E., Egorushkin, V.E., Surikova, N.S., and Pochivalov, Yu.I., Shear Bands as Translation-Rotation Mode of Plastic Deformation in Solids under Alternate Bending, *Mater. Sci. Eng. A*, 2017, vol. 703, pp. 451–460.